NIKHEF

NATIONAAL INSTITUUT VOOR KERNFYSICA EN HOGE-ENERGIEFYSICA

NIKHEF-H/86-1

High statistics inclusive ϕ meson production at SPS energies

H.Dijkstra[1], R.Bailey[6], E.Belau[5], T.Bohringer[3], M.Bosman[3], V.Chabaud[3], C.Damerell[6], C.Daum[1], G.de.Rijk[1], S.Gill[6], A.Gillman[6], R.Gilmore[2], Z.Hajduk[4], C.Hardwick[1], W.Hoogland[1], B.Kisielewski[4], B.D.Hyams[3], R.Klanner[5], S.Kwan[2], U.Kotz[3], G.Lutjens[5], G.Lutz[5], J.Malos[2], W.Manner[5], E.Neugebauer[5], H.Palka[4], M.Pepe[6], J.Richardson[6], K.Rybicki[4], H.J.Seebrunner[5], U.Stierlin[5], R.J.Tapper[2], H.G.Tiecke[1], M.Turala[4], G.Waltermann[5], S.Watts[6], P.Weilhammer[3], F.Wickens[6], L.W.Wiggers[1], A.Wylie[5] and T.Zeludziewicz[4]

The ACCMOR Collaboration

Abstract: Inclusive ϕ meson production has been measured for 100 GeV/c and 200 GeV/c incident π^-, $\bar{p}$ and K^-, and for 120 GeV/c and 200 GeV/c incident π^+, p and K^+, using a Be target. A total of 630,000 ϕ mesons has been recorded in the kinematic range $0 < x_F < 0.4$. Presented are the differential cross sections $d\sigma/dx_F$ and $d\sigma/dp_T^2$. The longitudinal momentum distributions show that the strange valence quarks of the incident K mesons play an important role in ϕ meson production, even at small x_F. The decay angular distribution of the ϕ meson is evaluated in the Gottfried – Jackson frame and is expressed in the elements of the density matrix. There is a small but significant $\cos^2\theta_{GJ}$ dependence for small p_T, which decreases for increasing p_T.

To be submitted to Zeitschrift fur Physik C

---

1) NIKHEF – H, Amsterdam, The Netherlands
2) University of Bristol, Bristol, U.K
3) CERN, Geneva, Switzerland
4) Institute of Nuclear Physics, Cracow, Poland
5) Max Planck Institute fur Physik, Munich, Fed. Rep. Germany
6) Rutherford Appleton Laboratory, Chilton, Didcot, U.K.

1. Introduction

This paper describes a high statistics experiment studying the inclusive reaction

$$\text{hadron} + \text{Be} \rightarrow \quad \phi(1020) + \text{anything}$$
$$\phi \rightarrow K^+ + K^-$$

in 100 GeV/c, 120 GeV/c and 200 GeV/c hadron interactions.

In previous experiments the ACCMOR collaboration has made a systematic study of the inclusive production of ϕ mesons [1] – [3]. The data were successfully interpreted in terms of a parton fusion model in which in particular the fusion of strange quarks plays an important role. This model explains naturally the observed enhanced production of strange particles in conjunction with the ϕ meson as well as the different shapes of the differential cross sections $d\sigma/dx_F$ for incident π mesons, protons and K mesons. In order to test this parton fusion model in more detail and possibly extract the momentum distribution functions for strange quarks in the interacting hadrons, a significant increase in statistics as well as a larger x_F range than previously accessible ($0. < x_F < 0.2$) was called for. This experiment was carried out in the summer of 1982 and yielded over 630,000 ϕ mesons in the kinematical range $0 < x_F < 0.4$ [4].

This paper is organized as follows. In chapter 2 the ACCMOR spectrometer is described. We give a description of the on – line event selection and of the acceptance corrections. The invariant mass distributions are shown in chapter 3 together with the transverse and longitudinal momentum distributions. The decay angular distribution is expressed in the elements of the density – matrix and is given in paragraph 3.5. The confrontation of the data with models which attempt to describe inclusive ϕ meson production are presented in a paper [5].

2. The Experiment

2.1 The spectrometer

The data were obtained with the NA11 spectrometer at the CERN SPS during the summer of 1982. Two differential Cherenkov counters were positioned in the beam line to identify incident particles. The trajectory of the incident beam is measured with a precision of σ(horizontal) = 25 μm and σ(vertical) = 6 μm at the 20 mm long Be target by six silicon microstrip detectors (BMSD). The apparatus used for the experiment is a single arm open spectrometer (figure 1) with two successive large aperture magnets, with a field of 0.902 Tm (MNP33) and 2.058 Tm (BBC).

The scintillator counter immediately behind the target (I − counter) is used in the trigger logic to define an inelastic interaction. The I − counter is followed by a system of six silicon microstrip detectors (VMSD) [6] which measure charged particle trajectories upstream of the first magnet. The measurement of the trajectories of the charged particles downstream of the MNP33 magnet is performed with a system of large drift chambers [7] with an efficiency of 98% and 0.17 mm resolution for perpendicularly incident tracks.

Those charged particles which traverse the part of the spectrometer behind the BBC magnet are identified with the threshold Cherenkov hodoscopes C_2 and C_3. Various gas fillings are used for the different beam momenta in the inclusive ϕ experiment. Table 1 lists the gases and the corresponding momentum thresholds for pions, kaons and protons. The Cherenkovs are operated at atmospheric pressure.

The two Cherenkovs C_2 and C_3, the scintillator hodoscopes MA and MB and the proportional chambers P31, P32 and P33 (figure 1) are used on − line to trigger on events which contain at least two kaon candidates. The elements of MA and MB match the elements of C_2 and C_3 respectively. Table 2 lists the parameters of the detectors used in the on − line trigger.

2.2 The trigger

The inclusive ϕ trigger consists of two stages. The first stage selects events with at least two oppositely charged kaon candidates downstream of the last magnet. The second stage makes use of a micro processor system to calculate the invariant mass of the kaon pairs and select ϕ meson candidates.

2.2.1 First stage trigger

The first stage selection of events uses a system of scintillator counters upstream of the target (not shown in figure 1) to signal beam particles which traverse the target. An inelastic interaction (INT) is defined by requiring a pulse height corresponding to at least two minimum ionizing particles in the interaction counter I and no signal in the D_2 – counter.

To select events which contain a ϕ meson decaying into K^+K^-, the trigger makes use of the typical signature of this decay, i.e. the small transverse momentum of each K meson with respect to the line of flight of the ϕ meson of at most 127 MeV/c. This ensures that the magnets will bend oppositely charged K mesons to opposite sides of the $x = 0$ symmetry plane of the spectrometer, provided that the transverse momentum of the ϕ meson itself is not too large. This condition defines the first stage trigger (M_ϕ):

$$M_\phi = INT \cdot \Sigma_{left}(MA.\overline{C_2} + MB.C_2.\overline{C_3}) \geq 1 \cdot \Sigma_{right}(MA.\overline{C_2} + MB.C_2.\overline{C_3}) \geq 1$$

In this expression $MA.\overline{C_2}$ represents the condition of a signal in an element of scintillator hodoscope MA without observing light in the corresponding cell of C_2. This condition selects K mesons with momenta below the K threshold of Cherenkov C_2 (see table 1 for the thresholds of the Cherenkovs), while π mesons with momenta larger than the π threshold of C_2 will be rejected. Inefficiencies of C_2 will result in an increase in the number of accepted π mesons, but will not reduce the acceptance for kaons in this momentum window.

The condition $MB.C_2.\overline{C_3}$ demands a signal in an element of hodoscope MB with no light in the matching C_3 cell and light in the corresponding cell of C_2. This condition is fulfilled for K mesons with momenta between the K thresholds of C_2 and C_3. Here an inefficiency of C_2 will result in a loss

of kaons in this momentum window. The multiplicity on the left side of the x = 0 plane (Σ_{left}) as well as the multiplicity on the right side (Σ_{right}) is required to be larger than zero.

The M_ϕ trigger restricts the momentum range of the K mesons that will be accepted. In particular those K mesons having a momentum larger than the K threshold of C_3 are not accepted by the trigger.

2.2.2 Second stage trigger

The final on − line selection is performed by the second stage trigger, which is based on the Fast Amsterdam Multi Processor (FAMP) system. The FAMP system and its design philosophy are extensively described elsewhere [8]. A detailed description of the system as it is used in the experiment can be found in [9]. It uses three FAMP units; one supervisor and two slaves. Each one consists of a FAMP module, two 32 Kbyte memory modules and a data buffer.

The FAMP system calculates the momenta of the K meson candidates flagged by the $MA.\overline{C}_2$ and $MB.C_2.\overline{C}_3$ coincidence using the information of the five proportional chamber planes $P31_{ab}$, $P32_{ab}$ and P33, the field integrals of the spectrometer magnets MNP and BBC and taking the target centre as origin.

The momenta of the particles are determined from the MWPC planes with $+7.125^0$ and -7.125^0 wire inclinations separately. The data from these planes are processed by the two slave processors in parallel. They check whether the MWPC hits are correlated with the pattern of the $MA.\overline{C}_2$ and $MB.C_2.\overline{C}_3$ coincidence of the first stage trigger. When such a correlation exists, hits in the P31 and P32 planes are combined which yield a momentum in the range imposed by the Cherenkov thresholds. If either of the slaves does not find a track candidate, the event is rejected, else the supervisor processor scans the two sets of momenta determined by the two views for equal values. If such a pair is found the processor searches for a correlated hit in P33, and performs a more accurate check of the correlation with the $MA.\overline{C}_2$ or $MB.C_2.\overline{C}_3$ coincidences.

For a K^+K^- pair with an invariant mass below 1050 MeV/c^2, the ratio of the K meson momenta is in the range 0.5 to 2. As soon as two particles with opposite polarity are found which satisfy this ratio of momenta, their invariant mass is calculated for the K^+K^- hypothesis. When no K^+K^- invariant

mass is found to be smaller than 1150 MeV/c^2 the event is rejected. The FAMP accepts 4% of the M_ϕ triggers.

The mean reconstruction time for an accepted event is 750 μs, for all events it is 450 μs. The second stage trigger accepts about 20% more events than the off−line analysis program does if similar selection criteria are applied. This is mainly due to ghost tracks found by the FAMP reconstruction program.

At regular intervals during data taking all events, both accepted and rejected, which are processed by the FAMP system are registered, in order to determine the efficiency of the second stage trigger system. This efficiency is calculated by comparing the decision taken by the FAMP system with the result from the off−line reconstruction program. The total efficiency of the second stage trigger is 70.2±0.5% for the low momentum runs (100, 120 GeV/c) and 73±2% for the high momentum runs (200 GeV/c). The inefficiency is mainly due to the MWPCs, which have an efficiency of 81.7% for detecting two tracks in all five planes, corresponding to an average efficiency of 98% per plane.

The efficiency varies with the momentum of the K mesons. For events where both K mesons have a momentum close to the π threshold of C_2 it is 63% while for events with K momenta in the range of the K threshold of C_2 it is 77%. The momentum dependence of the efficiency is incorporated in the computation of the acceptance. The effective gain in the number of ϕ mesons recorded per unit time obtained by the second stage trigger is about seven.

2.3 Acceptance

Inclusive $\phi \longrightarrow K^+K^-$ events will be lost due to the limited geometrical acceptance of the spectrometer, the decay or interaction of the K mesons, and trigger and reconstruction inefficiencies. A Monte Carlo procedure is used to calculate the acceptance accounting for these losses. Events are generated at random according to the following distributions : the ϕ mass is chosen according to a Breit−Wigner resonance with M_ϕ = 1019.5 MeV/c^2 and a full width of 4.2 MeV/c^2 ; the kinematical variables are taken for a $(1-|x|_F)^4.e^{-3p_T^2}$ dependence, where x_F is the Feynman variable for the longitudinal

momentum and p_T is the transverse momentum of the ϕ at production ; the decay angular distribution is isotropic in the Gottfried Jackson system with decay parameters $\cos\theta_{GJ}$ and ϕ_{GJ}; realistic distributions for beam shape and interaction point in the target are used.

The Monte Carlo events have to fulfil the same requirements as the real data, i.e. a K meson with a momentum smaller (larger) than the K threshold of C_2 is required to pass one of the elements of MA (MB) which is used in the trigger. For these K mesons the C_2 (C_3) cell is required to register no hit, so no loss due to an inefficient C_2 (C_3) cell can occur. However, the kaon could still be lost if the cell is illuminated by another particle with a momentum above its threshold. This last effect is simulated by mixing the hit pattern of the Cherenkovs from real events in the Monte Carlo events.

For kaons with a momentum larger than the K threshold of C_2, the C_2 cell should register the presence of light. The efficiency curve for C_2 is determined using π mesons from V^0 – decay. The efficiency curve is extrapolated to the K meson threshold of C_2 by multiplying the momentum with the ratio between the K and the π mass.

Figure 2 shows the acceptance for the 100 GeV/c run as a function of x_F and p_T^2. The total acceptance for ϕ mesons decaying into K^+K^- is typically 4%.

The acceptance has two maxima in the x_F projection, which correspond with the contributions to the trigger from the two Cherenkov counters C_2 and C_3.

3. Results

3.1 Data sets

We have collected data for various incident beam particles at a number of different beam momenta. Table 3 lists beam momentum, type of beam particle and the nanobarn equivalent for the various data sets: ten subsamples with the ϕ trigger at 100,120 and 200 GeV/c and two at 175 GeV/c with a minimum bias trigger from the same run as used for the study of $K^{*0}(890)$ production [10]. The nanobarn equivalent is given per nucleon per event, where we take a linear dependence of the ϕ production cross

section on the atomic weight A ($\sigma(A) = A^{\alpha}\sigma(A=1)$, with $\alpha = 1$). This is based on a measurement of inclusive ϕ production on H_2 and Be targets yielding $\alpha = 1.04 \pm 0.04$ [3] while a measurement using Be and Ta gave $\alpha = 0.88 \pm 0.02$ [11]. The nanobarn equivalent includes acceptance corrections which do not depend on the event kinematics, e.g. beam attenuation, trigger and reconstruction efficiencies, the branching ratio for $\phi \longrightarrow K^+K^-$,etc.. This gives rise to a correction factor 0.33 to 0.36 with an error of about 6% for the various data sets. It yields an overall scale error of about 6% in the differential cross sections.

3.2 The K^+K^- invariant mass distributions

Figure 3 a – l shows the K^+K^- invariant mass distributions for the various subsamples of the ϕ trigger. The number of ϕ mesons in each of the subsamples is determined by a fit using a Breit – Wigner resonance folded with a Gaussian distribution for the experimental resolution to represent the ϕ mass enhancement, superimposed on a second degree polynomial to account for the background. The data are fitted over the mass range $995 < M_{K^+K^-} < 1045$ MeV/c^2 in 1 MeV/c^2 bins. The free parameters in the fits are N_ϕ the number of ϕ mesons, M_ϕ the central mass of the ϕ meson , σ_{exp} the experimental mass resolution at the ϕ mass and the parameters defining the background polynomial. The width of the ϕ meson (Γ_ϕ) is fixed at the nominal value given by the PDG [12] i.e. $\Gamma_\phi = 4.2$ MeV/c^2. The results are listed in table 3 and are shown in figure 3. In the 100 GeV/c incident π^- data also Γ_ϕ was left as a free parameter. This fit yielded $\Gamma_\phi = 4.45 \pm 0.06$ MeV/c^2 and $\sigma_{exp} = 1.16 \pm 0.03$ MeV/c^2 with a correlation coefficient of -82%. The value obtained for the ϕ mass is consistent with the value of 1019.5 ± 0.1 MeV/c^2 given by the PDG [12].

The results are not very sensitive to the shape of the background. When a third degree polynomial background is used instead of one of second degree to parameterize the background N_ϕ changes by less than 0.1%. A change in the mass range over which the fit is performed affects the results by not more than 1%.

3.3 The transverse momentum distributions

Figure 2 shows that the acceptance for ϕ mesons falls off rapidly for increasing p_T^2. To obtain the differential cross section as a function of p_T^2 integrated over the whole x_F, $\cos\theta_{GJ}$ and φ_{GJ} ranges one should ideally determine the number of ϕ mesons in small four dimensional volumes spanned by the kinematical variables, for instance p_T^2, x_F, $\cos\theta_{GJ}$ and φ_{GJ}, weigh the ϕ mesons with the acceptance in that volume and project the data onto p_T^2. However the number of events per four dimensional volume becomes too small to determine the number of ϕ mesons and the number of background events separately. In order to determine nevertheless a p_T^2 distribution the above procedure is applied to two dimensional areas in the x_F and p_T^2 space for a realistic $d\sigma/d\Omega_{GJ}$ distribution.

The decay angular distributions of the ϕ meson appear to have a weak $\cos^2\theta_{GJ}$ dependence (see chapter 3.5), with a negligible φ_{GJ} dependence. In the acceptance calculations the $\cos\theta_{GJ}$ behaviour is represented by $dN/d\cos\theta_{GJ} \propto 1. + 0.15\cos^2\theta_{GJ}$ and the φ_{GJ} dependence is taken to be isotropic, which is the average over our data. The acceptance as a function of p_T^2 is rather insensitive to the chosen $\cos\theta_{GJ}$ distribution. An isotropic distribution in $\cos\theta_{GJ}$ increases the overall cross section by $\approx$1%, and does not change the shape of the $d\sigma/dp_T^2$ distribution.

The number of ϕ mesons in each (x_F, p_T^2) interval is obtained by making a fit to the K^+K^- mass spectrum in that interval as described in the previous chapter, with the mass of the ϕ meson fixed to a value of 1019.4 MeV/c^2. It was found that the coefficient of the quadratic term of the polynomial describing the background does not show a significant variation as a function of p_T^2 or x_F. This parameter was fixed at the value obtained by fitting the total K^+K^- spectrum.

For $p_T^2 < 500$ (MeV/c)^2 the differential cross section $d\sigma/dp_T^2$ in each x_F interval is well described by an exponential

$$d\sigma/dp_T^2 \propto e^{-bp_T^2} \qquad (3.3-1)$$

For the four data samples with the largest statistics b has been determined as a function of x_F, in the interval $p_T^2 < 500$ (MeV/c)^2. The results are shown in figure 4. The average values of b over the x_F range considered are 3.2±0.1, 3.0±0.1, 3.3±0.1 and 3.2±0.1 for the incident π^-, K^-, π^+ and p data respectively. They are indicated as a dashed line in figure 4.

A decrease in $< p_T >$ for $x_F \to 0$, the so-called seagull effect [13] should show an increase in b for decreasing x_F. The data shows no significant x_F dependence of the slope parameter b.

In order to determine the $d\sigma/dp_T^2$ distributions integrated over x_F we use the parameterization :

$$d\sigma/dx_F \propto (1 - x_F)^n$$

All data sets are integrated over the same x_F interval $0. < x_F < 0.45$ in order to obtain the correct relative normalization. Then, the K^+K^- spectra are fitted per p_T^2 interval. The number of ϕ mesons thus determined are corrected for acceptance losses using the aforementioned parameterizations of x_F and of the decay angular distributions of the ϕ meson. The sensitivity to the value of n in the parameterization of the x_F distribution is small. For example when the value of n = 4.0, determined for the 100 GeV/c incident π^- data is changed to n = 4.4 the value of b is reduced by 2%.

The $d\sigma/dp_T^2$ distributions are given in figures 5 and 6 for low and high momentum beams respectively. The smooth lines represent the best fits to the data with the parameterization (3.3 – 1). The slope parameters b are listed in table 4 for two different p_T^2 ranges. The x_F intervals from which statistically significant data are obtained are indicated in table 4. Other inclusive ϕ experiments [1] [3] [14] – [17] have measured comparable values for the slope parameter b. The results of table 4 show that for values of $p_T^2 > 0.5$ $(GeV/c)^2$ the distributions become flatter indicating that in order to obtain a proper fit to the data over a large p_T^2 range a one parameter fit may be insufficient.

3.4 The longitudinal momentum distributions

The longitudinal momentum distributions ($d\sigma/dx_F$) of the ϕ meson, integrated over all other kinematics parameters, have been determined by the procedure described in the previous chapter. The number of ϕ mesons in subsequent x_F intervals has been determined by fitting the corresponding K^+K^- invariant mass distributions. The acceptance for each x_F bin has been calculated by using the $d\sigma/dp_T^2$ parameterization (3.3 – 1), with the values of b as determined for each subsample. The average decay angular distribution is assumed to be given by $d^2\sigma/d\cos\theta_{GJ}d\varphi_{GJ} \propto 1. + 0.1\cos^2\theta_{GJ}$, as before.

The sensitivity of the results for a variation in these input parameters is small. Taking an isotropic decay angular distribution has no effect; changing slope parameter b from b = 3.0 to b = 3.2 for the 100 GeV/c incident π^- data does not affect the shape of the $d\sigma/dx_F$ distribution but leads to a 3.5% reduction in the absolute cross section.

The Lorentz invariant differential cross section is given by

$$f(x_F) = \frac{1}{\pi} \int \frac{E^*}{p^*_{max}} \frac{d^2\sigma}{dx_F dp_T^2} dp_T^2$$

where E^* is the energy of the ϕ meson and p^*_{max} its maximum longitudinal momentum in the overall centre of mass system. As was described in section 5, the absolute cross sections per nucleon have been obtained using linear A – dependence. The results on $d\sigma/dx_F$ and $f(x_F)$ are tabulated in table 5. The invariant cross sections are also shown in figures 7 and 8. In these figures also results from other experiments are included.

The errors indicated are statistical only. Typical systematic errors in the determination of the nanobarn equivalents are estimated to be of the order of 10%.

The shape of the distributions obtained in different experiments and at different energies appear to be reasonably consistent. The absolute normalization shows large discrepancies. In particular the data previously obtained by the ACCMOR collaboration at 93 GeV/c [1] and 100 GeV/c [3] are systematically lower by a factor of about two. We have no explanation for this. The cross section measured in the minimum bias 175 GeV/c data sample and the cross sections measured by several bubble chamber experiments [14] [15] [17] are consistent with the data of the present experiment. A possible source of error in the absolute normalization of our data could be a lack in understanding of our second stage trigger. We have therefore separately analyzed the data used for monitoring the second stage trigger (see section 2.3), where the trigger conditions are similar to the conditions used by references [1] and [3] in the x_F range $0.05 < x_F < 0.2$. Table 6 lists the values obtained for the differential cross section $d\sigma/dx_F$ using the monitor data with 100 GeV/c incident π^-. This cross section obtained is in agreement with the cross section obtained for the total data sample, hence the addition of the second stage trigger can not account for the discrepancy in the cross sections.

Comparison of the results for the various incident particles confirms the observation made in previous experiments, i.e. the incident $\pi^{\pm}$, p and $\bar{p}$ cross sections are comparable in size, while the incident p and $\bar{p}$ distributions decrease somewhat faster with increasing x_F than the incident $\pi^{\pm}$ data. The incident $K^{\pm}$ invariant cross section increases with increasing x_F in the x_F range $0. < x_F < 0.5$, and is comparable in size with the incident $\pi^{\pm}$, p and $\bar{p}$ cross sections at $x_F \approx 0$.

Figure 9 shows for this experiment the differential cross section for ϕ production for the interval $0.1 < x_F < 0.3$ as a function of s, the centre of mass energy squared. Here the error bars include a systematic error of 10%. Incident π, p and K are indicated with o, □ and Δ respectively. The cross section for incident K mesons in this x_F region is two times larger than the cross section for incident π and p, the latter two being comparable in amplitude. The cross section does not show a significant s – dependence. A ln(s) dependence would result in a 13% increase of the cross section in the range $s = 200$ GeV^2 to $s = 400$ GeV^2, i.e. an increase of the order of the systematical error.

3.5 The decay angular distributions of the φ meson

The decay angular distribution $I(\cos\theta,\varphi)$ of a spin 1 particle strongly decaying into two spin 0 particles, i.e. $\phi \rightarrow K^+ K^-$, can be written in the general form [18]

$$I(\cos\theta,\varphi) \propto \sum_{mn} Y_1^m(\theta,\varphi)\, \rho_{mn}\, Y_1^{n*}(\theta,\varphi), \qquad m,n = -1,0,1$$

where Y_1^j are spherical harmonics and ρ_{mn} denote the elements of the density matrix ρ. Here we will evaluate the distribution in the Gottfried – Jackson system. Parity conservation requires the ρ matrix to have the form [19]

$$\rho = \begin{pmatrix} \rho_{11} & \rho_{10} & \rho_{1,-1} \\ \rho_{10}^* & 1-2\rho_{11} & -\rho_{10}^* \\ \rho_{1,-1} & -\rho_{10} & \rho_{11} \end{pmatrix} \qquad (3.5-1)$$

where ρ_{11} and $\rho_{1,-1}$ are real. In terms of the ρ parameters the decay angular distribution can be written as

$$I(\cos\theta_{GJ},\varphi_{GJ}) = C\{\rho_{11} + (1-3\rho_{11})\cos^2\theta_{GJ} - \rho_{1,-1}\sin^2\theta_{GJ}\cos 2\varphi_{GJ} - \sqrt{2}\mathrm{Re}\rho_{10}\sin 2\theta_{GJ}\cos\varphi_{GJ}\} \qquad (3.5-2)$$

where C is a normalization factor. The number of expected events (N_i^{exp}) in an interval $\Delta\Omega_i$ around $(\cos\theta_{GJ},\varphi_{GJ})_i$ is related to $I(\cos\theta_{GJ},\varphi_{GJ})$ by

$$N_i^{exp} = A_i(\cos\theta_{GJ},\varphi_{GJ})\,\Delta\Omega_i\,I_i(\cos\theta_{GJ},\varphi_{GJ}) \qquad (3.5-3)$$

where $A_i(\cos\theta_{GJ},\varphi_{GJ})$ is the average acceptance in interval $\Delta\Omega_i$ and $I_i(\cos\theta_{GJ},\varphi_{GJ})$ is the mean value of the decay angular distribution in the same interval. The ρ parameters are determined by a χ^2 minimalization, where χ^2 is defined as

$$\chi^2 = \Sigma \frac{(N_i^{exp} - N_i^{obs})^2}{\sigma_i^2} \qquad (3.5-4)$$

where N_i^{obs} is the number of observed events in interval $\Delta\Omega_i$ and σ_i is the standard deviation in $(N_i^{exp} - N_i^{obs})$.

We have studied the p_T dependence of the density matrix elements integrated over the x_F range covered by the experiment. For this the data is split into 5 equal p_T intervals in the range $0. < p_T < 1.$ GeV/c. In every p_T interval the data are subdivided in 64 $\Delta\Omega_i$ intervals, corresponding to 8 $\cos\theta_{GJ}$ and 8 φ_{GJ} intervals and a fit is made to the K^+K^- mass spectra to determine the number of ϕ mesons. From this we obtain the number of ϕ mesons (N_i^{obs}) and the number of background events in the mass range $995 < M_{K^+K^-} < 1045$ MeV/c^2 separately.

In every volume of p_T and $\Delta\Omega$ the acceptance is determined with a Monte Carlo program. The density matrix elements are obtained by substituting (3.5 – 2) and (3.5 – 3) in equation (3.5 – 4) and minimizing the χ^2 with ρ_{mn} and the normalization constant C as free parameters.

Results for the 100 GeV/c incident π^- data for two p_T intervals which are representative for the general behaviour of the fits are shown in figures 10 and 11. In figure 10 the $\cos\theta_{GJ}$ distributions are plotted for the events with $p_T < 200$ MeV/c as a function of φ_{GJ}. The smooth curve is $I(\cos\theta_{GJ},\varphi_{GJ})$ fitted to the 64 measured points. In this fit both $\rho_{1,-1}$ and $Re\rho_{10}$ are about equal to 0., while ρ_{11} is different from 1/3, giving the distribution a $1.+\beta\cos^2\theta_{GJ}$ shape, with $\beta=(1-3\rho_{11})/\rho_{11}\cong 0.22$ (see equation (3.5−2)). Figure 11 shows the φ_{GJ} distributions for the events with $600 < p_T < 800$ MeV/c as a function of $\cos\theta_{GJ}$. A fit to these data gives $\rho_{11}\cong 1/3$. Both $\rho_{1,-1}$ and $Re\rho_{10}$ are different from 0., giving φ_{GJ} dependent distributions. Figure 12 shows the values of ρ_{11}, $\rho_{1,-1}$ and $Re\rho_{10}$ as a function of p_T for the six data samples where the statistics is sufficiently large over the whole p_T range to permit this analysis.

To demonstrate that the p_T dependence of the ρ matrix elements is indeed connected with the ϕ meson and not with the background, the analysis, using the spin 1 density matrix, is independently performed for the background in the ϕ mass region. For the acceptance calculations the $M_{K^+K^-}$ distribution of the background is assumed to be flat for $995 < M_{K^+K^-} < 1045$ MeV/c^2, and the x_F dependence is determined in a manner analogous to that used for to the x_F dependence of the ϕ mesons. We emphasize that no attempt is made to determine the spin of the background, we just assume that the non−resonant K^+K^- pair is in a spin 1 state. The results are shown in figure 12.

The ρ parameters lie within a volume of which the surface is given by

$$\det(\rho) = 0 \qquad (3.5-5)$$

except for two points. Expression (3.5−5) gives a surface of degree three in the ρ_{11}, $\rho_{1,-1}$ and ρ_{10} space and the allowed volume is the convex domain for which the determinant is positive limited by this surface which contains the origin. For the data from the 100 GeV/c incident K^- and the 17 GeV/c incident p beams the ρ_{mn} values of the background for $800 < p_T < 1000$ MeV/c fall far outside their allowed region and are not plotted in figure 12. This might indicate that the description of the non−resonant K^+K^- pair in terms of a spin 1 state only is too crude an approximation.

Table 7 lists the measured values of the density matrix elements for the ϕ mesons. The results presented in figure 12 indicate a common trend for the p_T dependence of the ρ matrix elements irrespective of the incident particle or momentum. Combining all the data gives the results listed in table 7 and shown in figure 13.

A possible $\cos^2\theta_{GJ}$ dependence of the ϕ meson has been observed by Sixel et al. [16] in data at 10 and 16 GeV/c integrated over all x_F and p_T. However the statistical significance is poor and the data cannot exclude an isotropic $\cos\theta_{GJ}$ distribution. Our data indicates a significant $\cos^2\theta_{GJ}$ term in the decay angular distribution at small p_T, which decreases for increasing p_T. This effect has also been observed for K^{*+} and K^{*0} production at 32 GeV/c [20] and 70 GeV/c [21] incident K^+.

4. Conclusions

We have measured inclusive ϕ meson production for 100 GeV/c and 200 GeV/c incident π^-, p and K^-, and 120 GeV/c and 200 GeV/c π^+, p and K^+. The trigger limits the x_F range of the observed 630,000 ϕ mesons to $0. < x_F < 0.4$.

The ϕ meson transverse momentum distributions are described by a single exponential in the range $0 < p_T^2 < 500$ (MeV/c)^2. The slope parameter has no significant x_F dependence.

The ϕ production cross section at $x_F \approx 0$ is rather independent of the incident particle,but the ϕ meson longitudinal momentum distributions for incident K mesons are much harder than for incident π mesons, protons and antiprotons. This reflects the importance of the strange valence quark of the K meson in the ϕ [illegible] production mechanism. The $d\sigma/dx_F$ for incident protons and antiprotons is somewhat softer than for incident π mesons, which indicates that the partons of the proton and antiproton which contribute to ϕ meson production carry less momentum than the corresponding partons of the π meson. The soft longitudinal momentum spectrum of the ϕ meson in pN interactions, together with the negligible difference in the cross sections for $pN \to \phi + X$ and $pN \to \phi + X$, indicates that the OZI inhibited light quark fusion plays an insignificant role in inclusive ϕ meson production.

The ϕ meson decay angular distribution in the Gottfried – Jackson frame shows a small but significant $\cos^2\theta_{GJ}$ dependence, which decreases for increasing p_T, irrespective of the incident particle. The ϕ_{GJ} dependence tends to increase for increasing p_T.

Acknowledgments

The contribution of the SPS crew, and of the SPS Experimental Area group are acknowledged for their invaluable services. We also wish to thank the technical staff of the participating laboratories for the excellent equipment which they have constructed for the NA11 spectrometer.

Finally we would like to thank C. Ponting and E. van Herwynen for their help in preparing this paper.

References

[1] C. Daum et al., Nucl. Phys. B186 (1981) 205

[2] C. Daum et al., Phys. Lett. 98B (1981) 313

[3] C. Daum et al., Z. Phys. C – Particles and Fields 18 (1983) 1

[4] H. Dijkstra, Ph. D. thesis, NIKHEF – H, Amsterdam, 1985

[5] H. Dijkstra et al., NIKHEF – H86/3, submitted to Z.Phys.C

[6] B. Hyams et al., Nucl. Instr. Meth. 205 (1983) 99

[7] C. Daum et al., Nucl. Instr. Meth. 176 (1980) 119

[8] L.O. Hertzberger, Comput. Phys. Commun. 26 (1982) 79

[9] C. Daum et al., Nucl. Instr. Meth. 217 (1983) 361

[10] R. Bailey et al., Z. Phys. C – Particles and Fields 24 (1984) 111

[11] R. Bailey et al., Z. Phys C – Particles and Fields 22 (1984) 125

[12] Review of Particle Properties, Rev. Mod. Phys. 56, No. 2, Part II (April 1984)

[13] G.W. van Apeldoorn et al., Nucl.Phys. B91 (1975) 1

[14] M. Barth et al., Phys. Lett. 117B (1982) 267

[15] P.V. Chliapnikov et al., Nucl. Phys. B176 (1980) 303

[16] P. Sinel et al., Nucl. Phys. B199 (1982) 381

[17] Yu. Arestov et al., Z. Phys. C – Particles and Fields 8 (1981) 283

[18] W. Koch, Proc. of the International School of Elementary Particle Physics, Herceg – Novi, edited by M. Nikolic (1968) 229

[19] K. Gottfried and J.D. Jackson, Nuovo Cim. 33 (1964) 309

[20] I.V. Ajinenko et al., Z. Phys. C – Particles and Fields 5 (1980) 177

[21] M. Barth et al., Nucl. Phys. B223 (1983) 296

Table 1:

Threshold and gas filling of the Cherenkov hodoscopes

Beam charge and momentum (GeV/c)	Cherenkov	gas	threshold (GeV/c) π	K	p
−100, +120	C_2	SF6	3.8	13.4	25.5
	C_3	N2, He	6.3	22.2	42.2
−200	C_2	N2	6.3	22.4	42.6
	C_3	N2, He	12.4	43.9	83.4
+200	C_2	N2	6.4	22.6	43.0
	C_3	N2, He	12.6	44.6	84.7

Table 2:

Parameters of spectrometer elements used in the trigger. Dimensions are given in the order x,y,z. A right handed coordinate system is used with the z−axis along the direction of the beam and the y−axis pointing upward. Wire inclinations are given with respect to the vertical (y−axis).

hodoscope	scintillator		Cherenkov	
	MA	MB	C_2	C_3
active area (m^2)	3.16× 1.1	4.× 1.62	3.03× 1.1	5.5× 1.6
number of rows	2	2	2	2
number of columns	12	8	11	10
threshold, gas	−	−	see table 1	

proportional chambers	P31	P32	P33
number of planes	2	2	1
active area (m^2)	1.9× 0.94	3.8× 0.94	3.8× 0.94
wire inclination	±7.125°	±7.125°	0°
wire pitch (mm)	1.985	1.985	2.
read−out pitch (mm)	1.985	3.969	8.
gas composition	75% argon(passing through methylal at 0°C) 24.5% isobutane, 0.5% freon		

spectrometer magnets	MNP33	BBC
field integral(T.m)	0.902	2.058

Table 3:

The various data sets of this experiment with parameters resulting from fits to the K^+K^- spectra. The errors given are statistical only. The nanobarn equivalent is given per nucleon and contains acceptance losses which do not depend on the event's kinematics, like the BR($\phi \to K^+K^-$).

beam GeV/c	incident particle	M_ϕ (MeV/c^2)	σ_{exp} (MeV/c^2)	N_ϕ	nanobarn equivalent
100	π^-	1019.41±0.01	1.28±0.02	270577±1053	0.058±0.004
	$\bar{p}$	1019.36±0.04	1.25±0.06	24574±343	0.60±0.04
	K^-	1019.43±0.02	1.35±0.03	72191±325	0.46±0.03
120	π^+	1019.40±0.02	1.30±0.03	121878±717	0.14±0.01
	p	1019.35±0.02	1.32±0.04	78524±622	0.19±0.02
	K^+	1019.44±0.05	1.41±0.09	9728±184	2.7±0.2
175	π^-	1019.39±0.14	1.54±0.2	5981±360	16.2±2.0
	K^-	1019.38±0.08	1.20±0.2	6229±240	40.6±4.5
200	π^-	1019.43±0.01	1.40±0.05	28548±339	0.57±0.04
200	π^+	1019.30±0.19	1.84±0.31	919±64	17.3±1.2
	p	1019.37±0.04	1.39±0.06	22095±317	0.72±0.05
	K^+	1019.68±0.14	1.23±0.22	995±51	27.8±1.9

Table 4:

Slope parameter b obtained from fitting the $d\sigma/dp_T^2$ distributions to expression (3.3 – 1) for two different ranges in p_T^2. The x_F interval indicates in which x_F range statistically significant data is available.

Beam GeV/c	incident particle	x_F range	b $(GeV/c)^{-2}$ $0. < p_T^2 < 0.5$	b $(GeV/c)^{-2}$ $0.5 < p_T^2 < 1.$
100	π^-	0.00 – 0.41	3.1 ± 0.1	2.8 ± 0.1
	$\bar{p}$	0.03 – 0.39	3.2 ± 0.2	2.9 ± 0.3
	K^-	0.03 – 0.40	2.9 ± 0.1	3.0 ± 0.1
120	π^+	0.01 – 0.33	3.2 ± 0.1	2.8 ± 0.1
	p	0.01 – 0.33	3.0 ± 0.1	2.8 ± 0.2
	K^+	0.00 – 0.31	3.1 ± 0.15	2.6 ± 0.3
200	π^-	0.03 – 0.39	3.3 ± 0.2	2.4 ± 0.2
200	π^+	0.03 – 0.39	3.6 ± 0.5	2.2 ± 1.0
	p	0.02 – 0.41	3.2 ± 0.2	2.7 ± 0.3
	K^+	0.03 – 0.33	3.2 ± 0.4	3.1 ± 0.8
Beam GeV/c	**incident particle**	**x_F range**	**b $(GeV/c)^{-2}$ $0. < p_T^2 < 1.0$**	**b $(GeV/c)^{-2}$ $1.0 < p_T^2 < 5.0$**
175	π^-	0. – 1.	2.6 ± 0.2	1.4 ± 0.2
	K^-	0. – 1.	2.2 ± 0.2	1.2 ± 0.1

Table 5:

Differential cross section $d\sigma/dx_F$ and the Lorentz invariant $f(x_F)$ per nucleon using linear A−dependence. The errors are statistical only.

beam GeV/c	incident particle	x_F interval	$d\sigma/dx_F$ (μb)	$f(x_F)$ (μb)
100	π^-	0.00 − 0.04	864. ± 88.	46.7 ± 4.8
		0.04 − 0.06	784. ± 44.	43.9 ± 2.4
		0.06 − 0.08	716. ± 33.	41.6 ± 1.9
		0.08 − 0.10	679. ± 29.	41.3 ± 1.8
		0.10 − 0.12	630. ± 26.	40.3 ± 1.7
		0.12 − 0.14	568. ± 24.	38.5 ± 1.6
		0.14 − 0.16	508. ± 21.	36.5 ± 1.5
		0.16 − 0.18	466. ± 19.	35.5 ± 1.5
		0.18 − 0.20	411. ± 17.	33.2 ± 1.4
		0.20 − 0.22	372. ± 16.	31.9 ± 1.3
		0.22 − 0.24	357. ± 15.	32.4 ± 1.4
		0.24 − 0.26	302. ± 13.	29.0 ± 1.2
		0.26 − 0.28	275. ± 11.	27.8 ± 1.2
		0.28 − 0.30	250. ± 11.	26.7 ± 1.1
		0.30 − 0.32	234. ± 10.	26.3 ± 1.1
		0.32 − 0.34	207. ± 9.	24.4 ± 1.1
		0.34 − 0.36	159. ± 7.	19.7 ± 0.9
		0.36 − 0.38	147. ± 7.	19.1 ± 0.9
		0.38 − 0.41	117. ± 7.	16.0 ± 1.0
100	$\bar{p}$	0.03 − 0.06	1078. ± 109.	59.7 ± 6.0
		0.06 − 0.08	937. ± 67.	54.3 ± 3.9
		0.08 − 0.10	784. ± 46.	47.6 ± 2.8
		0.10 − 0.12	774. ± 41.	49.5 ± 2.6
		0.12 − 0.14	578. ± 30.	39.1 ± 2.0
		0.14 − 0.16	511. ± 26.	36.7 ± 1.9
		0.16 − 0.18	452. ± 23.	34.4 ± 1.8
		0.18 − 0.20	416. ± 22.	33.6 ± 1.8
		0.20 − 0.22	325. ± 18.	27.8 ± 1.6
		0.22 − 0.24	316. ± 17.	28.7 ± 1.6
		0.24 − 0.26	255. ± 14.	24.4 ± 1.4
		0.26 − 0.28	209. ± 12.	21.1 ± 1.2
		0.28 − 0.30	167. ± 10.	17.8 ± 1.1
		0.30 − 0.32	151. ± 10.	17.0 ± 1.1
		0.32 − 0.34	143. ± 9.	16.8 ± 1.1
		0.34 − 0.36	95. ± 9.	11.7 ± 1.1
		0.36 − 0.39	88. ± 8.	11.6 ± 1.0
100	K^-	0.03 − 0.06	1011. ± 95.	56.1 ± 5.3
		0.06 − 0.08	896. ± 57.	52.0 ± 3.3
		0.08 − 0.10	890. ± 47.	54.1 ± 2.8
		0.10 − 0.12	893. ± 42.	57.2 ± 2.7
		0.12 − 0.14	871. ± 39.	59.0 ± 2.7
		0.14 − 0.16	818. ± 36.	58.7 ± 2.6
		0.16 − 0.18	810. ± 36.	61.7 ± 2.7
		0.18 − 0.20	780. ± 34.	63.0 ± 2.8
		0.20 − 0.22	797. ± 35.	68.3 ± 3.0
		0.22 − 0.24	781. ± 34.	70.9 ± 3.1

		0.24 – 0.26	760. ± 33.	73.0 ± 3.1
		0.26 – 0.28	745. ± 32.	75.5 ± 3.2
		0.28 – 0.30	740. ± 31.	79.0 ± 3.4
		0.30 – 0.32	776. ± 33.	87.1 ± 3.7
		0.32 – 0.34	761. ± 32.	89.7 ± 3.8
		0.34 – 0.36	700. ± 31.	86.6 ± 3.8
		0.36 – 0.38	674. ± 31.	87.2 ± 4.0
		0.38 – 0.40	705. ± 36.	95.4 ± 4.9
120	π^+	0.01 – 0.03	909. ± 92.	44.9 ± 4.6
		0.03 – 0.05	974. ± 54.	49.3 ± 2.8
		0.05 – 0.07	899. ± 42.	47.3 ± 2.2
		0.07 – 0.09	878. ± 38.	48.5 ± 2.1
		0.09 – 0.11	769. ± 33.	45.0 ± 1.9
		0.11 – 0.13	707. ± 30.	43.9 ± 1.9
		0.13 – 0.15	618. ± 26.	40.9 ± 1.7
		0.15 – 0.17	522. ± 22.	36.9 ± 1.6
		0.17 – 0.19	497. ± 21.	37.4 ± 1.6
		0.19 – 0.21	470. ± 20.	37.7 ± 1.6
		0.21 – 0.23	397. ± 17.	34.0 ± 1.5
		0.23 – 0.25	369. ± 16.	33.5 ± 1.5
		0.25 – 0.27	357. ± 16.	34.3 ± 1.5
		0.27 – 0.29	297. ± 14.	30.2 ± 1.4
		0.29 – 0.31	250. ± 13.	26.8 ± 1.4
		0.31 – 0.33	217. ± 14.	24.5 ± 1.6
120	p	0.01 – 0.04	1332. ± 105.	66.0 ± 5.2
		0.04 – 0.06	1096. ± 57.	56.3 ± 2.9
		0.06 – 0.08	917. ± 42.	49.3 ± 2.3
		0.08 – 0.10	841. ± 37.	47.7 ± 2.1
		0.10 – 0.12	710. ± 31.	42.7 ± 1.9
		0.12 – 0.14	631. ± 27.	40.4 ± 1.8
		0.14 – 0.16	537. ± 24.	36.7 ± 1.6
		0.16 – 0.18	428. ± 19.	31.2 ± 1.4
		0.18 – 0.20	384. ± 17.	29.9 ± 1.4
		0.20 – 0.22	322. ± 15.	26.6 ± 1.2
		0.22 – 0.24	277. ± 13.	24.4 ± 1.1
		0.24 – 0.26	257. ± 12.	24.0 ± 1.1
		0.26 – 0.28	203. ± 10.	20.1 ± 1.0
		0.28 – 0.30	163. ± 9.	17.1 ± 0.9
		0.30 – 0.33	116. ± 8.	12.9 ± 0.9
120	K^+	0.00 – 0.07	962. ± 83.	48.3 ± 4.2
		0.07 – 0.09	870. ± 68.	48.0 ± 3.8
		0.09 – 0.11	913. ± 60.	53.3 ± 3.5
		0.11 – 0.13	831. ± 52.	51.6 ± 3.2
		0.13 – 0.15	837. ± 51.	55.4 ± 3.3
		0.15 – 0.17	738. ± 47.	52.1 ± 3.3
		0.17 – 0.19	789. ± 49.	59.4 ± 3.7
		0.19 – 0.21	827. ± 47.	66.5 ± 3.8
		0.21 – 0.23	781. ± 43.	66.7 ± 3.7
		0.23 – 0.25	814. ± 44.	73.8 ± 4.0
		0.25 – 0.27	863. ± 46.	83.0 ± 4.4
		0.27 – 0.29	732. ± 43.	74.4 ± 4.4
		0.29 – 0.31	755. ± 53.	81.0 ± 5.7

175	π^-	0.00 – 0.10	970. ± 100.	42.3 ± 4.4
		0.10 – 0.20	540. ± 40.	33.8 ± 2.5
		0.20 – 0.30	260. ± 30.	23.2 ± 2.7
		0.30 – 0.40	130. ± 30.	15.4 ± 3.6
		0.40 – 0.50	60. ± 20.	8.9 ± 3.0
175	K^-	0.00 – 0.10	1590. ± 150.	69.3 ± 6.5
		0.10 – 0.20	900. ± 100.	56.4 ± 6.3
		0.20 – 0.30	820. ± 80.	73.2 ± 7.1
		0.30 – 0.40	650. ± 70.	77.1 ± 8.3
		0.40 – 0.50	510. ± 70.	75.9 ± 10.4
200	π^-	0.03 – 0.06	837. ± 77.	34.0 ± 3.1
		0.06 – 0.08	767. ± 54.	33.8 ± 2.4
		0.08 – 0.10	760. ± 50.	36.1 ± 2.4
		0.10 – 0.12	684. ± 44.	35.3 ± 2.3
		0.12 – 0.14	623. ± 40.	35.0 ± 2.3
		0.14 – 0.16	562. ± 37.	34.3 ± 2.2
		0.16 – 0.18	471. ± 32.	31.2 ± 2.1
		0.18 – 0.20	403. ± 28.	28.8 ± 2.0
		0.20 – 0.22	391. ± 27.	30.0 ± 2.1
		0.22 – 0.24	327. ± 23.	27.0 ± 1.9
		0.24 – 0.26	291. ± 21.	25.6 ± 1.9
		0.26 – 0.28	246. ± 18.	23.1 ± 1.7
		0.28 – 0.30	224. ± 17.	22.4 ± 1.7
		0.30 – 0.32	237. ± 17.	25.0 ± 1.8
		0.32 – 0.34	185. ± 14.	20.7 ± 1.6
		0.34 – 0.36	135. ± 12.	15.9 ± 1.4
		0.36 – 0.39	85. ± 10.	10.6 ± 1.2
200	π^+	0.03 – 0.10	1055. ± 118.	45.6 ± 5.1
		0.10 – 0.14	669. ± 77.	36.0 ± 4.2
		0.14 – 0.19	530. ± 58.	34.4 ± 3.7
		0.19 – 0.32	258. ± 29.	23.1 ± 2.6
200	p	0.02 – 0.06	1327. ± 117.	53.1 ± 4.7
		0.06 – 0.08	1072. ± 76.	47.2 ± 3.3
		0.08 – 0.10	1040. ± 68.	49.5 ± 3.2
		0.10 – 0.12	846. ± 55.	43.7 ± 2.9
		0.12 – 0.14	655. ± 44.	36.8 ± 2.4
		0.14 – 0.16	581. ± 39.	35.5 ± 2.4
		0.16 – 0.18	438. ± 31.	29.0 ± 2.1
		0.18 – 0.20	343. ± 27.	24.5 ± 1.9
		0.20 – 0.22	284. ± 22.	21.8 ± 1.7
		0.22 – 0.24	229. ± 19.	18.9 ± 1.6
		0.24 – 0.26	191. ± 16.	16.8 ± 1.4
		0.26 – 0.28	145. ± 14.	13.6 ± 1.3
		0.28 – 0.30	125. ± 12.	12.5 ± 1.2
		0.30 – 0.32	102. ± 10.	10.8 ± 1.0
		0.32 – 0.41	45. ± 8.	5.5 ± 1.0
200	K^+	0.03 – 0.11	1312. ± 140.	57.7 ± 6.2
		0.11 – 0.14	1050. ± 117.	57.8 ± 6.4
		0.14 – 0.20	741. ± 85.	49.0 ± 5.6
		0.20 – 0.25	906. ± 104.	73.5 ± 8.4
		0.25 – 0.33	569. ± 63.	56.8 ± 6.2

Table 6:

Differential cross section $d\sigma/dx_F$ for monitor data of 100 GeV/c incident π^-.

x_F interval	number of ϕ mesons	$d\sigma/dx_F$ (μb)
0.05 – 0.10	142 ± 27	622 ± 118
0.10 – 0.15	401 ± 35	560 ± 49
0.15 – 0.20	523 ± 48	538 ± 49
0.20 – 0.25	269 ± 33	330 ± 40
0.25 – 0.30	245 ± 24	278 ± 27
0.30 – 0.35	195 ± 26	242 ± 32
0.35 – 0.40	41 ± 14	124 ± 32

Table 7:

The ρ parameters.

incident beam GeV/c		p_T range GeV/c	ρ_{11}	$\rho_{1,-1}$	Re ρ_{10}
100	π^-	0.0 – 0.2	0.311 ± 0.003	-.002 ± 0.005	0.007 ± 0.004
		0.2 – 0.4	0.315 ± 0.003	-.001 ± 0.004	0.017 ± 0.003
		0.4 – 0.6	0.328 ± 0.003	0.023 ± 0.005	0.027 ± 0.003
		0.6 – 0.8	0.333 ± 0.004	0.036 ± 0.007	0.028 ± 0.005
		0.8 – 1.0	0.348 ± 0.007	0.012 ± 0.013	-.005 ± 0.009
100	K^-	0.0 – 0.2	0.310 ± 0.005	-.005 ± 0.008	0.012 ± 0.006
		0.2 – 0.4	0.313 ± 0.004	-.009 ± 0.006	0.008 ± 0.004
		0.4 – 0.6	0.336 ± 0.004	0.028 ± 0.007	0.032 ± 0.005
		0.6 – 0.8	0.331 ± 0.005	0.037 ± 0.009	0.019 ± 0.006
		0.8 – 1.0	0.327 ± 0.011	0.065 ± 0.018	-.023 ± 0.015
120	π^+	0.0 – 0.2	0.301 ± 0.005	-.009 ± 0.007	0.012 ± 0.006
		0.2 – 0.4	0.317 ± 0.003	-.001 ± 0.006	0.023 ± 0.004
		0.4 – 0.6	0.322 ± 0.004	0.019 ± 0.006	0.021 ± 0.004
		0.6 – 0.8	0.337 ± 0.006	0.022 ± 0.010	0.015 ± 0.007
		0.8 – 1.0	0.354 ± 0.010	0.014 ± 0.019	0.026 ± 0.013
120	p	0.0 – 0.2	0.308 ± 0.006	-.007 ± 0.009	0.026 ± 0.007
		0.2 – 0.4	0.311 ± 0.004	-.015 ± 0.007	0.014 ± 0.005
		0.4 – 0.6	0.327 ± 0.005	0.011 ± 0.008	0.028 ± 0.006
		0.6 – 0.8	0.338 ± 0.007	0.015 ± 0.013	0.022 ± 0.008
		0.8 – 1.0	0.325 ± 0.015	0.101 ± 0.029	-.018 ± 0.019
200	π^-	0.0 – 0.2	0.313 ± 0.008	0.007 ± 0.013	0.001 ± 0.010
		0.2 – 0.4	0.306 ± 0.006	0.010 ± 0.010	0.021 ± 0.007
		0.4 – 0.6	0.337 ± 0.007	0.026 ± 0.011	0.036 ± 0.008
		0.6 – 0.8	0.323 ± 0.009	0.009 ± 0.015	0.037 ± 0.010
		0.8 – 1.0	0.309 ± 0.017	0.031 ± 0.028	0.026 ± 0.019
200	p	0.0 – 0.2	0.285 ± 0.010	-.018 ± 0.015	0.001 ± 0.012
		0.2 – 0.4	0.298 ± 0.008	0.015 ± 0.012	0.026 ± 0.009
		0.4 – 0.6	0.304 ± 0.008	0.018 ± 0.013	0.035 ± 0.009
		0.6 – 0.8	0.308 ± 0.011	-.007 ± 0.019	0.023 ± 0.013
		0.8 – 1.0	0.322 ± 0.023	0.018 ± 0.041	0.013 ± 0.028
mean		0.0 – 0.2	0.307 ± 0.002	-.005 ± 0.003	0.011 ± 0.003
		0.2 – 0.4	0.312 ± 0.002	-.002 ± 0.003	0.017 ± 0.002
		0.4 – 0.6	0.327 ± 0.002	0.021 ± 0.003	0.028 ± 0.002
		0.6 – 0.8	0.331 ± 0.002	0.023 ± 0.004	0.024 ± 0.003
		0.8 – 1.0	0.336 ± 0.005	0.037 ± 0.008	0.002 ± 0.006

Figure Captions

Figure 1: Top view of the spectrometer showing target, magnets (MNP33, BBC), drift chambers (DC2, DC3A, DC3B, DC3C), Cherenkovs (C_2, C_3), multi wire proportional chambers (P31, P32 P33), the scintillation counter D_2 and scintillator hodoscopes (MA, MB). The inset shows a side view of the target region with twelve silicon microstrip detectors (BMSD, VMSD), Be target and interaction defining counter (I).

Figure 2: Acceptance for ϕ mesons decaying into K^+K^-.

Figure 3: The K^+K^- invariant mass spectra. The incident beam particle and its momentum (in GeV/c) are given in each plot. Figures k and l are obtained using a minimum bias trigger.

Figure 4: The slope parameter b obtained from fitting the $d\sigma/dp_T^2$ distributions in $0. < p_T^2 < 500$ $(MeV/c)^2$ to the expression $e^{-bp_T^2}$, as a function of x_F for 100 GeV/c incident π^-,K^- and 120 GeV/c incident π^+ and p. The dashed lines are the b values averaged over x_F.

Figure 5: Differential cross section $d\sigma/dp_T^2$ for the low momentum incident beams. The data has been integrated over $0. < x_F < 0.45$. The solid lines represent fits to the data over the whole p_T range with expression $(3.3-1)$.

Figure 6: Differential cross section $d\sigma/dp_T^2$ for the high momentum incident beams. The data has been integrated over $0. < x_F < 0.45$, apart from the 175 GeV/c data, which is integrated over $0. < x_F < 1$. The solid lines represent fits to the data over the whole p_T range with expression $(3.3-1)$.

Figure 7: Lorentz invariant differential cross sections $f(x_F)$ per nucleon for incident π^-, $\bar{p}$ and K^-. The data is compared with other experiments using linear $A-$dependence. +, o, □: this experiment; Δ, ⊙: reference [1] □: reference [3] Δ: reference [17]. The incident particles are indicated in each plot.

Figure 8: Lorentz invariant differential cross sections $f(x_F)$ per nucleon for incident π^+, p and K^+. The data is compared with other experiments using linear $A-$dependence. +, o: this experiment; Δ: reference [1] □: reference [3] ⊙: reference [14] Δ: reference [15]. The incident particles are indicated in each plot.

Figure 9: The cross section $d\sigma/dx_F$ per nucleon as a function of s for $0.1 < x_F < 0.3$. Incident π, p and K are indicated with o, □ and Δ respectively.

Figure 10: $dN/d\cos\theta_{GJ}$ for 100 GeV/c incident π^- and $0. < p_T < 200$ MeV/c for 8 φ_{GJ} intervals. The smooth lines represent the best fit to the decay angular distribution $I(\cos\theta_{GJ},\varphi_{GJ})$.

Figure 11: $dN/d\varphi_{GJ}$ for 100 GeV/c incident π^- and $600 < p_T < 800$ MeV/c for 8 $\cos\theta_{GJ}$ intervals. The smooth lines represent the best fit to the decay angular distribution $I(\cos\theta_{GJ},\varphi_{GJ})$.

Figure 12: ρ_{11}, $\rho_{1,-1}$ and $Re\rho_{10}$ as function of p_T. The elements for the ϕ mesons are indicated with "+". The background is determined separately and the values of its elements are indicated with "o". The dashed line represents $\rho_{11} = 1/3$. The incident particles and their momentum are indicated above each plot.

Figure 13: The value of the ρ elements averaged over all incident particles and momenta. The dashed line represents $\rho_{11} = 1/3$. Symbols as in figure 12.

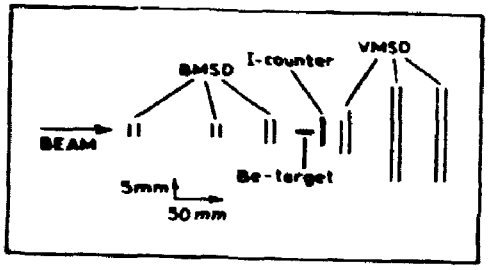

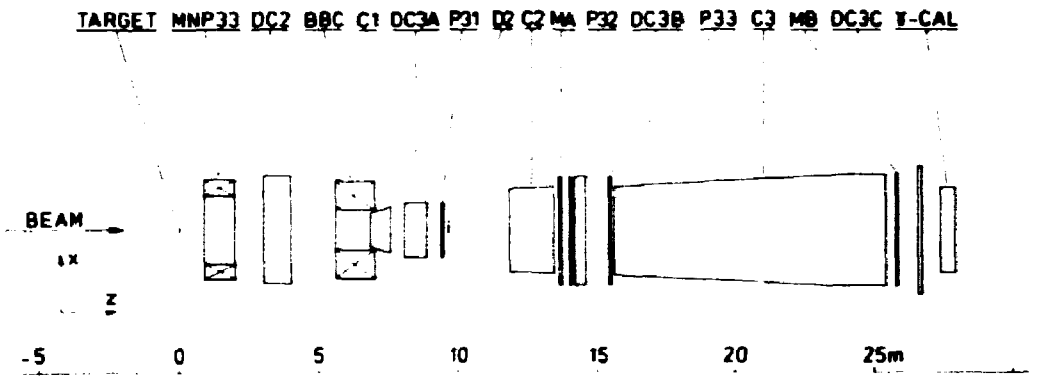

Figure 1.

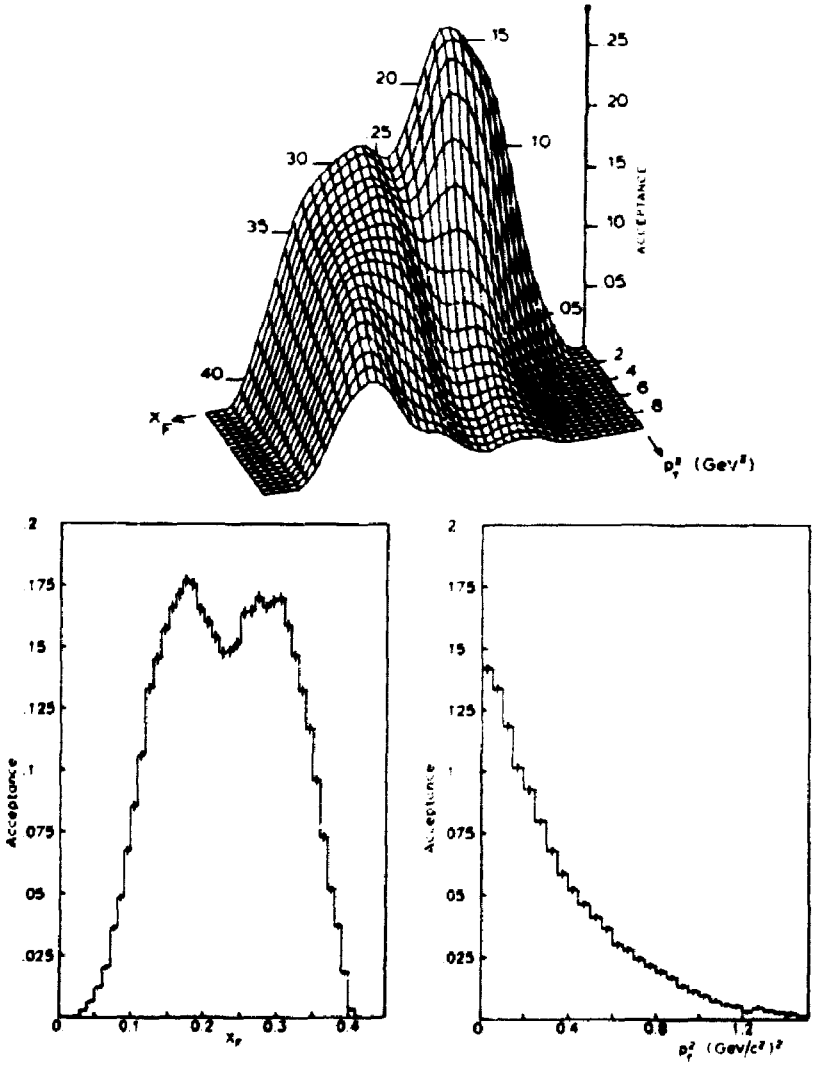

Figure 2.

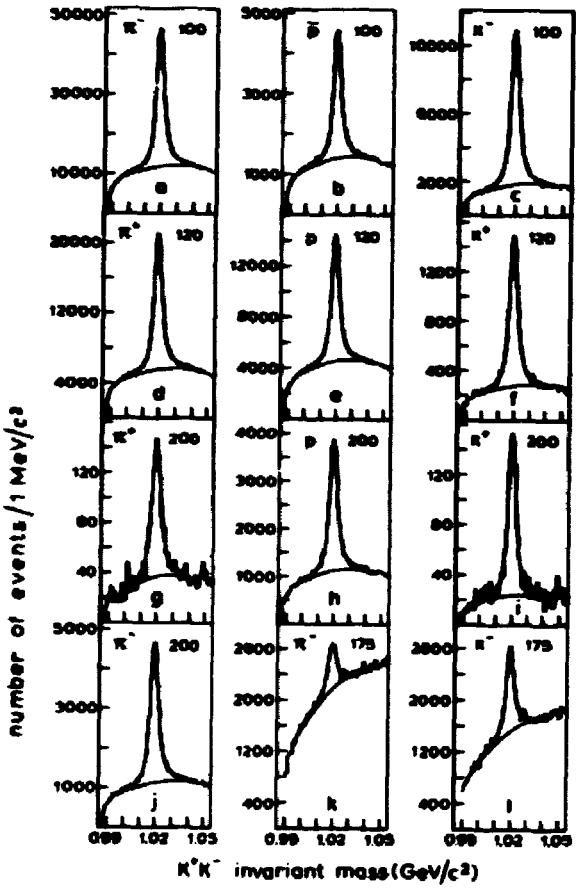

Figure 3.

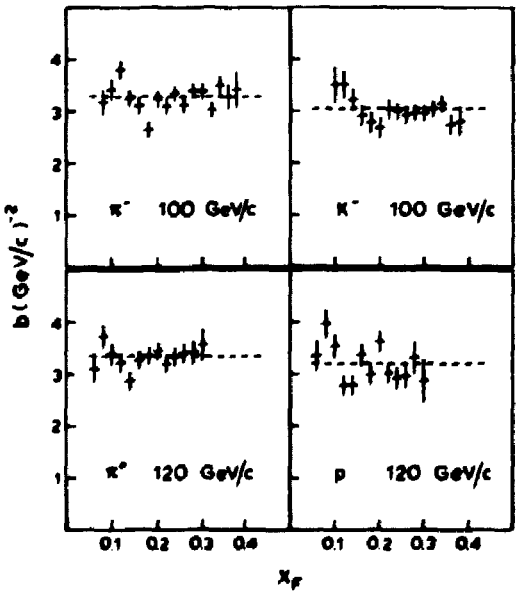

Figure 4.

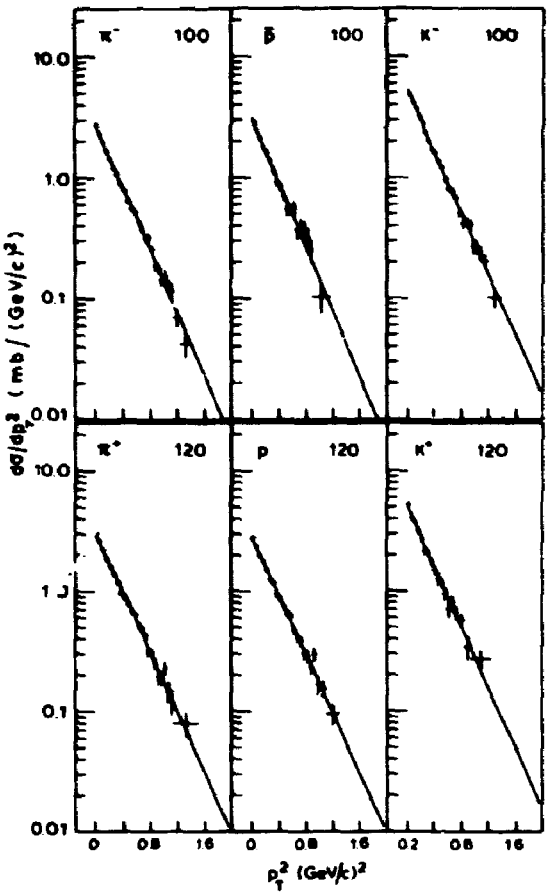

Figure 5.

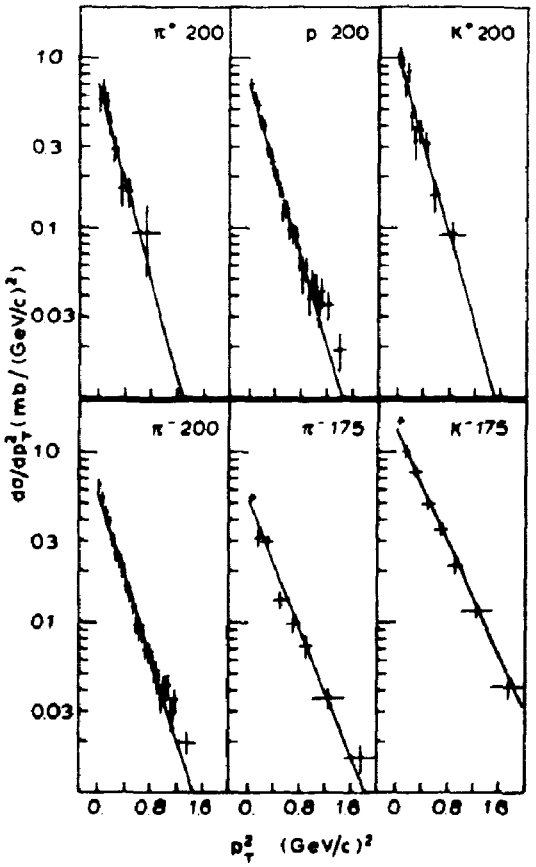

Figure 6.

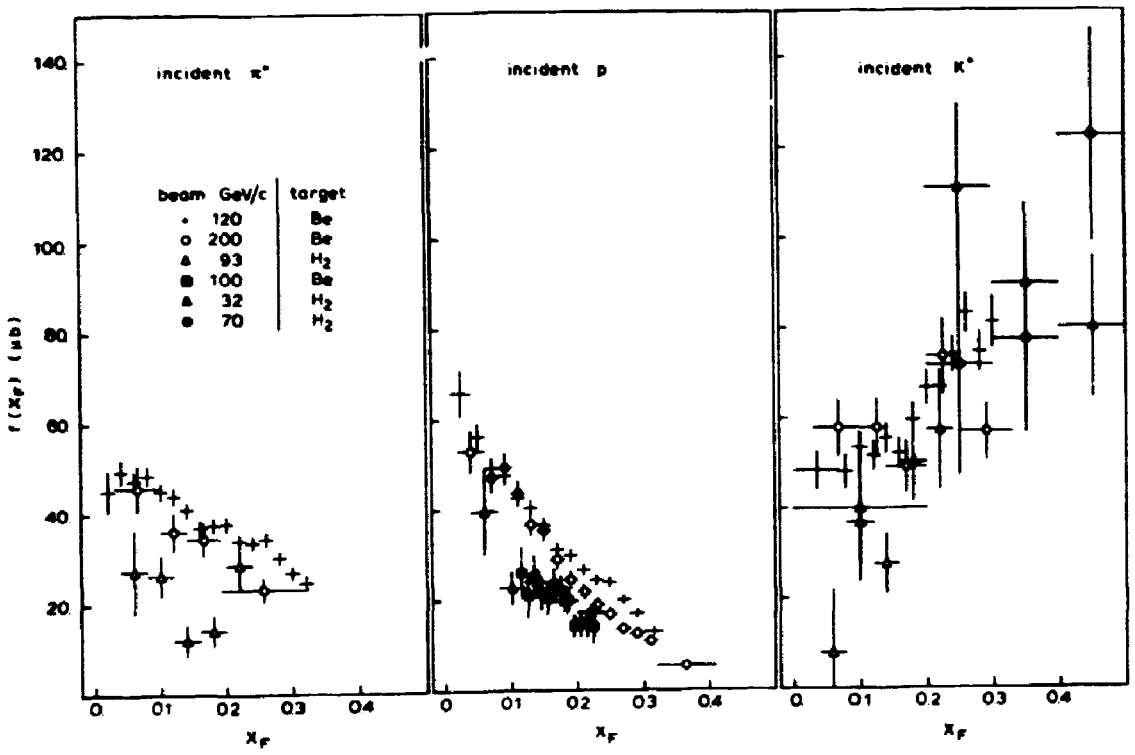

Figure 8.

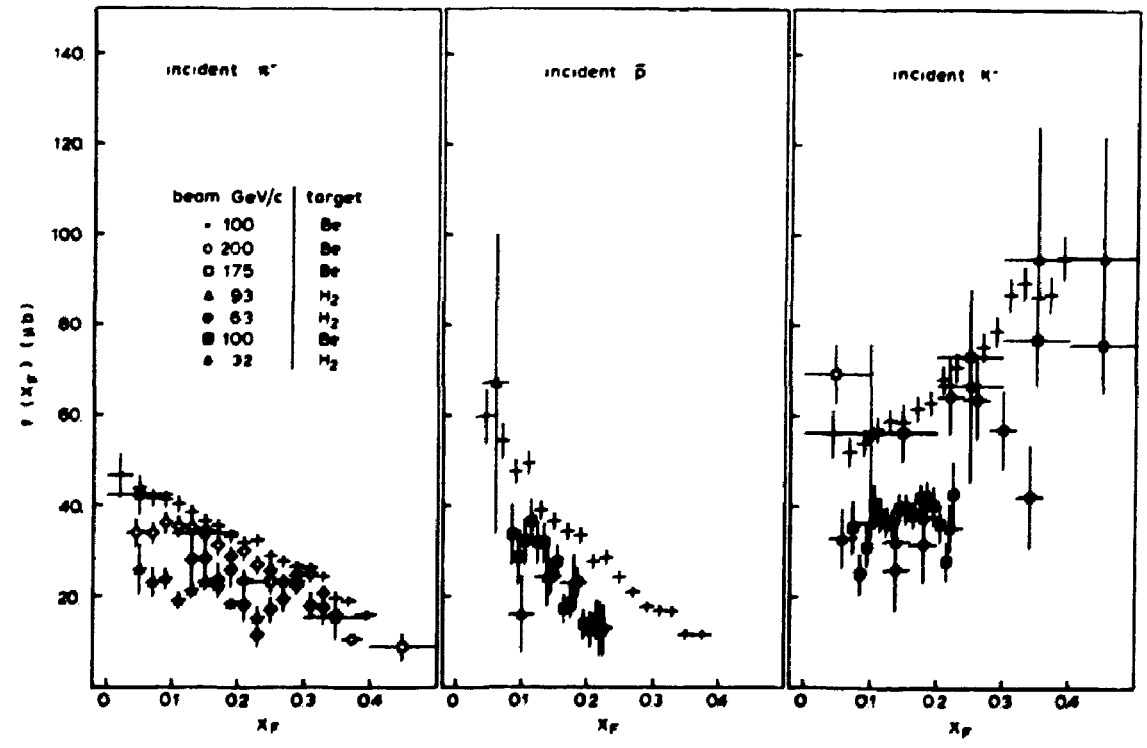

Figure 7.

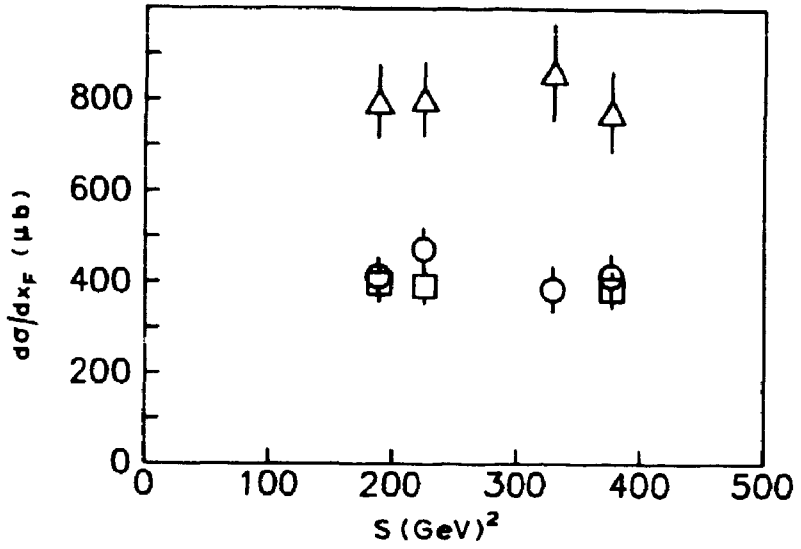

Figure 9.

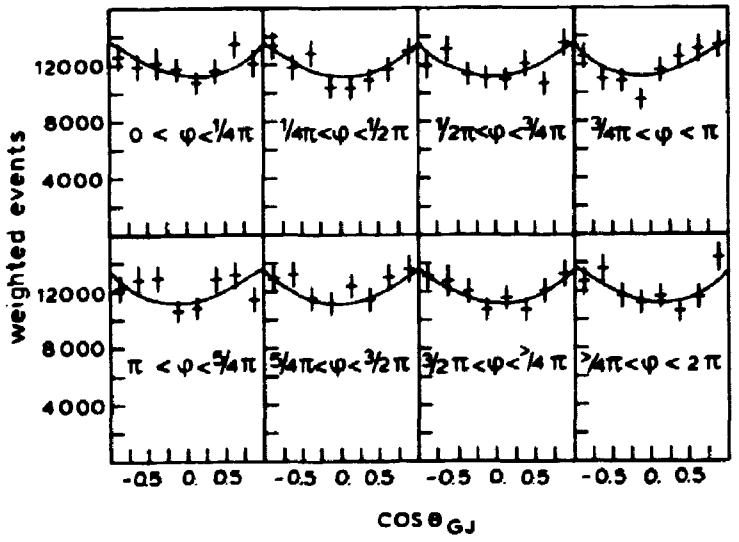

Figure 10.

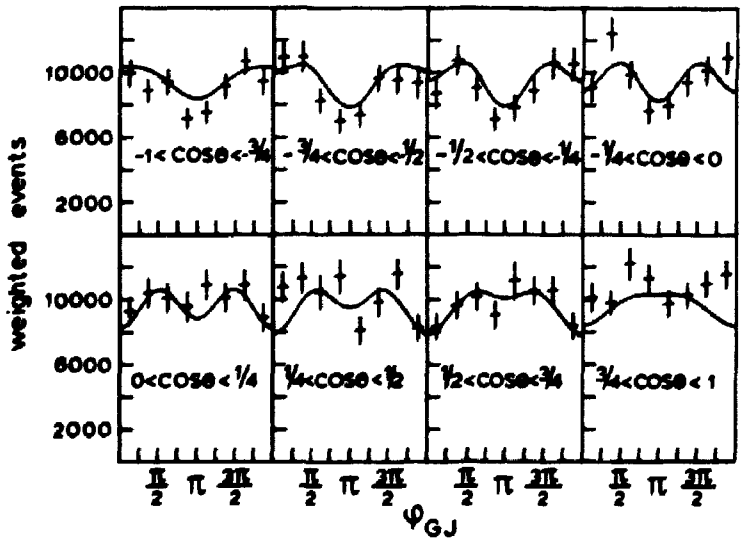

Figure 11.

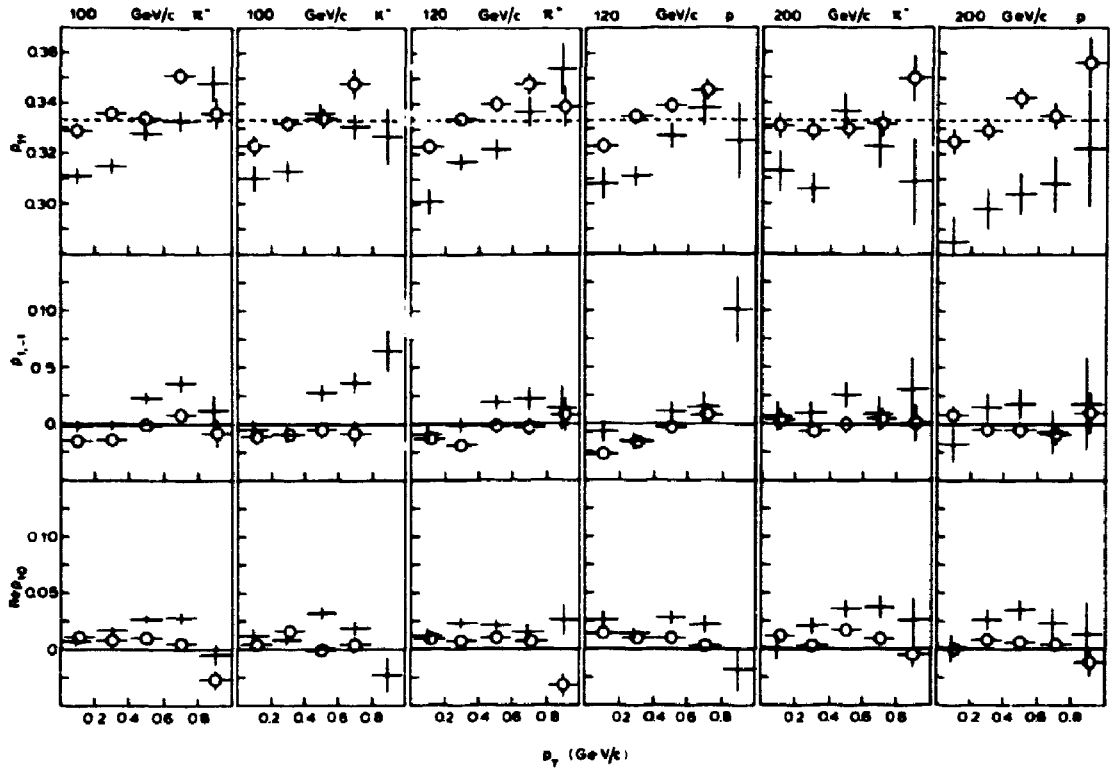

Figure 12.

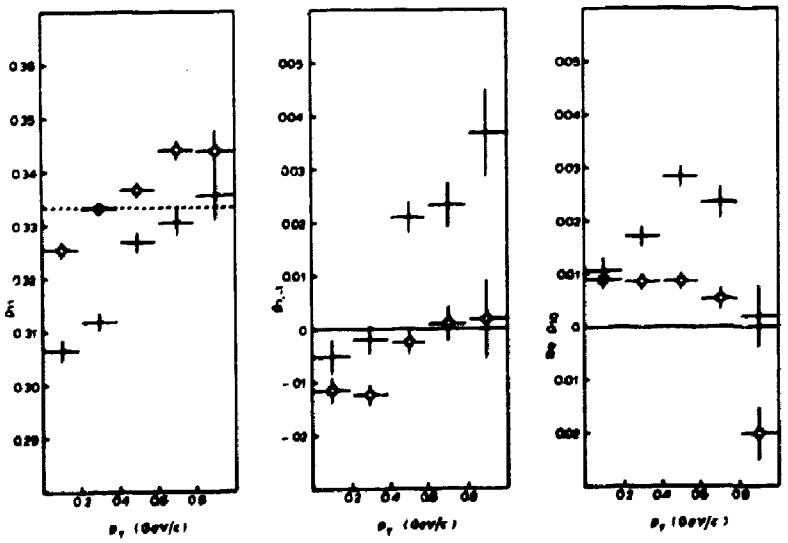

Figure 13.